DESY 97-41
HUP-EP-97-15
UFTP 440/1997

DESY 97-41
HUP-EP-97/15
UFTP 440/1997
hep-lat/9703014

hep-lat/9703014 21 Mar 97

# Pion and Rho Structure Functions from Lattice QCD

C. Best[1], M. Göckeler[1,2], R. Horsley[3], E.-M. Ilgenfritz[3], H. Perlt[4], P. Rakow[5], A. Schäfer[1], G. Schierholz[5,6], A. Schiller[4], S. Schramm[7]

[1] Institut für Theoretische Physik, Johann Wolfgang Goethe–Universität, D–60054 Frankfurt am Main, Germany

[2] Institut für Theoretische Physik, RWTH Aachen, D–52056 Aachen, Germany

[3] Institut für Physik, Humboldt-Universität, D–10115 Berlin, Germany

[4] Institut für Theoretische Physik, Universität Leipzig, D–04109 Leipzig, Germany

[5] Deutsches Elektronen-Synchrotron DESY, Institut für Hochenergiephysik and HLRZ, D–15735 Zeuthen, Germany

[6] Deutsches Elektronen-Synchrotron DESY, D–22603 Hamburg, Germany

[7] Gesellschaft für Schwerionenforschung GSI, D–64220 Darmstadt, Germany

**Abstract**

We calculate the lower moments of the deep-inelastic structure functions of the pion and the rho meson on the lattice. Of particular interest to us are the spin-dependent structure functions of the rho. The calculations are done with Wilson fermions and for three values of the quark mass, so that we can perform an extrapolation to the chiral limit.

# 1 Introduction

The deep-inelastic structure functions of nucleons and mesons are currently receiving a lot of attention, both experimentally and theoretically. It has become possible to compute these structure functions from first principles within the framework of lattice QCD [1, 2]. This allows a quantitative test of QCD which goes beyond perturbation theory. The basis of the calculation is the operator product expansion which relates the moments of the structure functions to forward hadron matrix elements of certain local operators. Lattice simulations of these matrix elements, combined with an appropriate calculation of the Wilson coefficients, can in principle provide complete information of the quark and gluonic structure of the hadronic states. The aim of this paper is to compute the structure functions of the pion and the rho meson. Following [2] we use Wilson fermions and work in the quenched approximation, where internal quark loops are neglected.

The pion structure function, which so far was extracted from measurements of the Drell-Yan lepton-pair production cross section [3], is directly being measured at HERA at present [4], and we expect that new data will become available soon. Using the techniques described in [5, 6], it should in principle be possible to measure the structure functions of the rho as well in the near future. Some of the spin-dependent structure functions, in particular, should be easy to separate from the dominant pion exchange process.

But even without having any experimental data to compare with, the internal structure of the rho meson is an interesting subject to study on the lattice. Besides the structure functions already known from the nucleon, one finds new structure functions that contain qualitatively new information which has no analog in the case of spin-$\frac{1}{2}$ targets [7]. We hope that this

investigation will lead to a better understanding of quark binding effects in hadrons.

The structure functions of the rho are also of interest for the interpretation of photoproduction and two-photon inclusive cross sections, as the photon has a substantial hadronic component which to a good approximation can be described by the rho meson.

For a spin-0 target like the pion, the kinematical framework is simpler than in the familiar nucleon case. The details for the case of a polarized spin-1 particle have been worked out by Hoodbhoy et al. [7]. The hadronic tensor, i.e. the imaginary part of the forward current-hadron scattering amplitude,

$$W^{\mu\nu}(p,q,\lambda,\lambda') = \frac{1}{4\pi}\int \mathrm{d}^4x\, e^{\mathrm{i}q\cdot x}\,\langle p,\lambda'|[j^\mu(x),j^\nu(0)]|p,\lambda\rangle \tag{1}$$

(with $\lambda$, $\lambda'$ labeling the polarization) decomposes into eight structure functions:

$$\begin{aligned} W_{\mu\nu} \;=\; & -F_1 g_{\mu\nu} + F_2\frac{p_\mu p_\nu}{\nu} - b_1 r_{\mu\nu} + \frac{1}{6}b_2(s_{\mu\nu}+t_{\mu\nu}+u_{\mu\nu}) + \frac{1}{2}b_3(s_{\mu\nu}-u_{\mu\nu}) \\ & + \frac{1}{2}b_4(s_{\mu\nu}-t_{\mu\nu}) + \mathrm{i}\frac{g_1}{\nu}\epsilon_{\mu\nu\lambda\sigma}q^\lambda s^\sigma \\ & + \mathrm{i}\frac{g_2}{\nu^2}\epsilon_{\mu\nu\lambda\sigma}q^\lambda(p\cdot q s^\sigma - s\cdot q p^\sigma) \quad , \end{aligned} \tag{2}$$

where $\nu = p\cdot q$, and $r_{\mu\nu}$, $s_{\mu\nu}$, $t_{\mu\nu}$, $u_{\mu\nu}$ are kinematical tensors [7] constructed from the momentum transfer $q$ and the polarization vector $\epsilon$. The latter satisfies $\epsilon\cdot p = 0$, $\epsilon^2 = -m^2$, and

$$s^\sigma = \frac{-\mathrm{i}}{m^2}\epsilon^{\sigma\alpha\beta\tau}\epsilon^*_\alpha\epsilon_\beta p_\tau \quad , \tag{3}$$

with $m$ being the hadron mass. Here $\epsilon^{\mu\nu\lambda\sigma}$ is the completely antisymmetric tensor with $\epsilon^{0123} = -1$.

The structure functions $F_1$, $F_2$, $g_1$, and $g_2$ play the same role as for a spin-$\frac{1}{2}$ target. In the parton model, the structure of the hadron can be described by the probability $q^m_\uparrow(x)$ ($q^m_\downarrow(x)$) of finding a quark with momentum fraction $x$ and spin up (down) along the direction of motion when the hadron is moving with infinite momentum and has spin projection $m = 0, \pm 1$. Symmetry implies

$$\begin{aligned} q^1_\uparrow(x) = q^{-1}_\downarrow(x), \qquad q^1_\downarrow(x) = q^{-1}_\uparrow(x) \quad , \\ q^0_\uparrow(x) = q^0_\downarrow(x) \quad , \end{aligned} \tag{4}$$

so there remain only three independent parton distribution functions $q^1_\uparrow(x)$, $q^1_\downarrow(x)$, and $q^0_\uparrow(x)$. In leading order, the single-flavor structure function $F_1^{(q)}(x)$ is one half of the probability to find a quark $q$ with momentum fraction $x$, and $F_2^{(q)}(x)$ obeys the Callan-Gross relation:

$$\begin{aligned} F_1^{(q)}(x) &= \frac{1}{3}\left(q^1_\uparrow(x) + q^1_\downarrow(x) + q^0_\uparrow(x)\right) \quad , \\ F_2^{(q)}(x) &= 2x F_1^{(q)}(x) \quad . \end{aligned} \tag{5}$$

In the complete structure function, $F_1^{(q)}(x)$ is weighted by the electric charge $Q_q$ of the quarks:

$$F_1(x) = \sum_q Q_q^2 F_1^{(q)}(x) \quad . \tag{6}$$

In the following, we will only specify single-flavor structure functions and omit the superscript $(q)$. For the mesons under consideration, the structure functions are identical for both flavors. The polarized structure function $g_1(x)$ gives the fraction of spin carried by quarks:

$$g_1(x) = \frac{1}{2}\left[q^1_\uparrow(x) - q^1_\downarrow(x)\right] \quad . \tag{7}$$

The structure function $g_2(x)$ does not have a parton model interpretation.

The structure functions $b_1(x)$, $b_2(x)$, $b_3(x)$, and $b_4(x)$ are particular to spin-1 targets as the kinematical factors in eq. (2) involve the target polarization vector to second order, a feature that does not occur for spin-$\frac{1}{2}$ targets. In parton model language $b_1(x)$ and $b_2(x)$ depend on the quark-spin averaged distributions $q^m = \frac{1}{2}(q^m_\uparrow + q^m_\downarrow)$ only:

$$b_1(x) = q^0(x) - q^1(x) \quad , \tag{8}$$

$$b_2(x) = 2x b_1(x) \quad . \tag{9}$$

Thus $b_1(x)$ and $b_2(x)$ measure the difference in parton distributions of an $m = 1$ and $m = 0$ target. This difference is due to the fact that in quantum field theory any Lorentz boost changes the particle content of a state. These changes differ for different spin orientations relative to the boost direction. For a model discussion of $b_1$ see e.g. [8].

The paper is organized as follows. In Sec. 2 we recall some results from the operator product expansion concerning the relevant operators and their

matrix elements. Sec. 3 describes the method we use to extract matrix elements from three-point functions. The lattice implementation of this method is discussed in Sec. 4. Sec. 5 is devoted to questions of normalization and renormalization. In Sec. 6 we discuss our results, and Sec. 7 presents our conclusions. Appendix A contains our conventions, Appendices B and C describe some technicalities. The reader who is not interested in the computational details may skip Secs. 3 and 4.

# 2 Operators and moments of the structure functions

The moments of structure functions can be related to the reduced matrix elements of certain local operators between pion or rho states. The local operators we consider are built from $\gamma$ matrices and covariant derivatives and have the general form in Minkowski space

$$\hat{O}^{(M)\mu_1\cdots\mu_n} = \frac{1}{2^{n-1}}\, G_{ff'}\, \bar{\psi}_f \gamma^{\mu_1} \mathrm{i}\overleftrightarrow{D}^{\mu_2} \ldots \mathrm{i}\overleftrightarrow{D}^{\mu_n} \psi_{f'} \quad , \tag{10}$$

$$\hat{O}_5^{(M)\mu_1\cdots\mu_n} = \frac{1}{2^{n-1}}\, G_{ff'}\, \bar{\psi}_f \gamma^{\mu_1}\gamma_5 \mathrm{i}\overleftrightarrow{D}^{\mu_2} \ldots \mathrm{i}\overleftrightarrow{D}^{\mu_n} \psi_{f'} \quad , \tag{11}$$

where $\psi$ is the quark field, and $G_{ff'}$ is a suitably chosen diagonal flavor matrix. The symmetrized derivative operators $\overleftrightarrow{D}$ are defined as

$$\overleftrightarrow{D} = \overrightarrow{D} - \overleftarrow{D} \quad . \tag{12}$$

For a spin-0 particle, the momentum vector $p$ is the only quantity the matrix element can depend on, and the reduced matrix element $v_n$ is defined by

$$\langle\vec{p}|\hat{O}^{(M)\{\mu_1\cdots\mu_n\}} - \text{traces}|\vec{p}\rangle = 2v_n\, [p^{\mu_1}\cdots p^{\mu_n} - \text{traces}] \quad . \tag{13}$$

The notation $\{\mu_1\cdots\mu_n\}$ denotes symmetrization in the indices $\mu_1$, $\mu_2$, ..., $\mu_n$. Expectation values of operators involving the $\gamma_5$ matrix vanish from symmetry considerations as the pion is a pseudoscalar particle.

For a spin-1 particle, the structure of the matrix elements is more complicated due to the polarization degrees of freedom. Now both types of operators contribute[1]:

$$\langle p,\lambda|\hat{O}^{(M)\{\mu_1\ldots\mu_n\}} - \text{traces}|p,\lambda\rangle \;=\; 2S\Big[a_n\, p^{\mu_1}\cdots p^{\mu_n}$$

[1]Note that we have corrected in (15) a misprint in [7].

$$+ d_n \left(\epsilon^{*\mu_1}(\vec{p},\lambda)\epsilon^{\mu_2}(\vec{p},\lambda) - \frac{1}{3}p^{\mu_1}p^{\mu_2}\right) p^{\mu_3}\cdots p^{\mu_n}\Big] \quad , \quad (14)$$

$$\langle p,\lambda|\hat{O}_5^{(M)\{\mu_1\ldots\mu_n\}} - \text{traces}|p,\lambda\rangle = \frac{2\mathrm{i}}{m^2}\, S\left[r_n\, \epsilon^{\rho\sigma\tau\mu_1}\epsilon^*_\rho(\vec{p},\lambda)\epsilon_\sigma(\vec{p},\lambda)p_\tau p^{\mu_2}\cdots p^{\mu_n}\right]. \quad (15)$$

$S$ denotes symmetrization in the indices $\mu_1$, ..., $\mu_n$ and removal of traces. The reduced matrix elements are $a_n$ for the polarization-averaged contribution, $d_n$ for the polarized contributions, and $r_n$ for the operators involving $\gamma_5$.

By performing an operator product expansion of (1), reduced matrix elements of local operators can be related to moments of the structure functions. We define the $n$-th moment of a function $f(x)$ as

$$M_n(f) = \int_0^1 x^{n-1} f(x)\,\mathrm{d}x \quad . \quad (16)$$

One then finds to leading order, which is twist two, the following representation of the moments of the pion structure functions:

$$\begin{aligned} 2M_n(F_1) &= C_n^{(1)}\, v_n \quad , \\ M_{n-1}(F_2) &= C_n^{(2)}\, v_n \quad ; \end{aligned} \quad (17)$$

for the rho structure functions one obtains [7]:

$$\begin{aligned} 2M_n(F_1) &= C_n^{(1)}\, a_n \quad , \\ M_{n-1}(F_2) &= C_n^{(2)}\, a_n \quad , \\ 2M_n(b_1) &= C_n^{(1)}\, d_n \quad , \\ M_{n-1}(b_2) &= C_n^{(2)}\, d_n \quad , \\ 2M_n(g_1) &= C_n^{(3)}\, r_n \quad , \end{aligned} \quad (18)$$

where $C_n^{(k)} = 1 + O(\alpha_s)$ are the Wilson coefficients of the operator product expansion. These relations hold for even $n$, except for the last one, which is valid for odd $n$. However, since we are calculating in the quenched approximation, we are allowed to make use of these formulas for all $n$ keeping in mind that our results can be meaningfully compared only with the non-singlet valence quark distribution.

In the case of the pion, the moments of the quark distribution are given by

$$\langle x^{n-1}\rangle = v_n \quad , \quad (19)$$

while for the rho they are related to the matrix elements $a_n$:

$$\langle x^{n-1} \rangle = a_n \quad . \tag{20}$$

# 3 Three-point functions and matrix elements

In order to calculate the reduced matrix elements on the lattice, we must calculate the expectation values of local operators of the form (10) and (11). To this end, we first need the connection between the Minkowski operators and those in Euclidean space. Defining Euclidean operators by

$$\hat{O}^{(E)}_{\mu_1 \cdots \mu_n} = G_{ff'} \frac{1}{2^{n-1}} \bar{\psi}_f \gamma^{(E)}_{\mu_1} \overleftrightarrow{D}^{(E)}_{\mu_2} \ldots \overleftrightarrow{D}^{(E)}_{\mu_n} \psi_{f'} \quad , \tag{21}$$

$$\hat{O}^{(E)5}_{\mu_1 \cdots \mu_n} = G_{ff'} \frac{1}{2^{n-1}} \bar{\psi}_f \gamma^{(E)}_{\mu_1} \gamma_5 \overleftrightarrow{D}^{(E)}_{\mu_2} \ldots \overleftrightarrow{D}^{(E)}_{\mu_n} \psi_{f'} \quad , \tag{22}$$

we obtain the following relation to the operators in Minkowski space:

$$\hat{O}^{(M)\mu_1 \cdots \mu_n} = (-)\,(-)^{n_4+n_5}\,(-\mathrm{i})^{n_{123}}\,\hat{O}^{(E)}_{\mu_1 \cdots \mu_n} \quad , \tag{23}$$

where $n_4$ is the number of time-like indices, $n_{123}$ the number of spatial indices, and $n_5 = 1$ if the operator carries a $\gamma_5$ matrix. For our Euclidean conventions, see Appendix A.

Lattice operators with the appropriate continuum behavior can be constructed from the Wilson fermion fields by considering their symmetry properties under the hypercubic group $H(4)$ [9]. The operators we have chosen and their relation to the reduced matrix elements are listed in Appendix B.

The required expectation values of our operators are extracted from ratios of two- and three-point functions. The three-point functions we consider are of the general form

$$\langle \eta(t, \vec{p})\, \mathcal{O}(\tau)\, \eta^\dagger(0, \vec{p}) \rangle \tag{24}$$

where $\eta(t, \vec{p})$ is the sink operator for a particle moving with momentum $\vec{p}$ in time slice $t$, and $\eta^\dagger(0, \vec{p})$ is the corresponding source at time slice $t = 0$. These operators are required to have the correct symmetry properties for the particles in question and their corresponding Hilbert space operators $\hat{\eta}(\vec{p})$ should create the desired particles from the vacuum with nonzero amplitude. $\mathcal{O}(\tau)$ represents the operator $\hat{O}$ whose expectation value is to be calculated.

For the pion we write

$$\langle 0 | \hat{\eta}(\pi; \vec{p}) | \pi; \vec{p} \rangle = \sqrt{Z_\pi} \quad , \tag{25}$$

while for the rho there are three different particle states and correspondingly three different operators arranged in a vector $\eta_i(\rho;t,\vec{p})$ that satisfy

$$\langle 0|\hat{\eta}_j(\rho;\vec{p})|\rho;\vec{p},\lambda\rangle = \sqrt{Z_\rho}\,\epsilon_j(\vec{p},\lambda) \tag{26}$$

up to lattice artifacts (see Appendix A for the definition of the polarization vectors $\epsilon_i$). The correlation function for the rho depends on the polarization vectors:

$$C_{jk} = \langle \eta_j(\rho;t,\vec{p})\,\mathcal{O}(\tau)\,\eta_k^\dagger(\rho;0,\vec{p})\rangle \quad . \tag{27}$$

In order to relate (27) to the matrix elements we are interested in, we express this correlation function in terms of traces involving the transfer matrix $\hat{S}$:

$$\begin{aligned}\langle \eta_j(\rho;t,\vec{p})\,\mathcal{O}(\tau)\,\eta_k^\dagger(\rho;0,\vec{p})\rangle &= \\ &= \begin{cases} \mathrm{tr}\left[\hat{S}^{T-t}\hat{\eta}_j(\rho;\vec{p})\hat{S}^{t-\tau}\hat{O}\hat{S}^{\tau}\hat{\eta}_k^\dagger(\rho;\vec{p})\right] & T\geq t\geq\tau\geq 0 \quad , \\ \mathrm{tr}\left[\hat{S}^{T-\tau}\hat{O}\hat{S}^{\tau-t}\hat{\eta}_j(\rho;\vec{p})\hat{S}^{t}\hat{\eta}_k^\dagger(\rho;\vec{p})\right] & T\geq\tau\geq t\geq 0 \quad . \end{cases}\end{aligned} \tag{28}$$

Here $T$ denotes the time extent of our lattice whose spacing is put equal to 1. Then we insert a complete set of orthonormal eigenstates of the transfer matrix. If the time differences are chosen sufficiently large, we can restrict ourselves to the lowest contributing states $|\vec{p},\lambda\rangle$, $\lambda$ labeling the three degenerate polarization states of the rho. For the first case in (28) one obtains

$$\begin{aligned} C_{jk}^{(1)} &= \sum_{\lambda\lambda'} \langle 0|\hat{\eta}_j(\rho;\vec{p})|\rho;\vec{p},\lambda\rangle\,\langle\rho;\vec{p},\lambda|\hat{O}|\rho;\vec{p},\lambda'\rangle\,\langle\rho;\vec{p},\lambda'|\hat{\eta}_k(\rho;\vec{p})|0\rangle\,e^{-Et} \\ &= Z_\rho \sum_{\lambda\lambda'} \epsilon_j(\vec{p},\lambda)\,\epsilon_k^*(\vec{p},\lambda')\,\langle\rho;\vec{p},\lambda|\hat{O}|\rho;\vec{p},\lambda'\rangle\,e^{-Et} \\ &= Z_\rho\, m^2\, T_{jk}\, e^{-Et} \quad , \end{aligned} \tag{29}$$

where $T_{jk}$ is the matrix element between Cartesian states,

$$T_{jk} = \frac{1}{m^2}\sum_{\lambda\lambda'} \epsilon_j(\vec{p},\lambda)\epsilon_k^*(\vec{p},\lambda')\langle\rho;\vec{p},\lambda|\hat{O}|\rho;\vec{p},\lambda'\rangle \quad . \tag{30}$$

In the second case, one finds an additional sign factor:

$$C_{jk}^{(2)} = (-1)^{n_4+n_5}\, Z_\rho\, m^2\, T_{jk}\, e^{-E(T-t)} \quad . \tag{31}$$

To calculate all $C_{jk}$ components for a given momentum would be expensive in computer time. Choosing the momentum in 1-direction, we have

restricted ourselves to the components $C_{33}$ and $C_{32}$. If $\langle \rho; \vec{p}, + | \hat{O} | \rho; \vec{p}, - \rangle = 0$ and $\langle \rho; \vec{p}, + | \hat{O} | \rho; \vec{p}, + \rangle = \langle \rho; \vec{p}, - | \hat{O} | \rho; \vec{p}, - \rangle$, then

$$\langle \rho; \vec{p}, + | \hat{O} | \rho; \vec{p}, + \rangle = T_{33} \quad , \qquad T_{32} = 0 \quad , \tag{32}$$

whereas for $\langle \rho; \vec{p}, + | \hat{O} | \rho; \vec{p}, + \rangle = - \langle \rho; \vec{p}, - | \hat{O} | \rho; \vec{p}, - \rangle$,

$$\langle \rho; \vec{p}, + | \hat{O} | \rho; \vec{p}, + \rangle = -\mathrm{i} T_{32} \quad , \qquad T_{33} = 0 \quad . \tag{33}$$

The latter case is relevant to spin-dependent operators. To satisfy

$$\langle \rho; \vec{p}, + | \hat{O} | \rho; \vec{p}, - \rangle = 0 \quad ,$$

it is sufficient that the operators commute with rotations in the plane transverse to $\vec{p}$. This has also motivated our choice of operators.

The factors that do not depend on the operator $\hat{O}$ can be eliminated by taking the ratio of (27) to another correlator, e.g. the two-point correlator

$$\begin{aligned} C(t) &= \sum_j \langle \eta_j(\rho; t, \vec{p})\, \eta_j^\dagger(\rho; 0, \vec{p}) \rangle \\ &= \sum_\lambda \Big[ \langle 0 | \hat{\eta}_j(\rho; \vec{p}) | \rho; \vec{p}, \lambda \rangle \, \langle \rho; \vec{p}, \lambda | \hat{\eta}_k^\dagger(\rho; \vec{p}) | 0 \rangle \, e^{-Et} \\ &\quad + \langle \rho; \vec{p}, \lambda | \hat{\eta}_j(\rho; \vec{p}) | 0 \rangle \, \langle 0 | \hat{\eta}_k^\dagger(\rho; \vec{p}) | \rho; \vec{p}, \lambda \rangle \, e^{-E(T-t)} \Big] \quad . \end{aligned} \tag{34}$$

Using the relations (26) and (73), this reduces to

$$C(t) = Z_\rho \, (2m^2 + E^2) \, \left( e^{-Et} + e^{-E(T-t)} \right) \quad . \tag{35}$$

We therefore arrive at the following relation between the ratio of a three- to a two-point correlation function and the expectation value of the corresponding operator, valid for $t \gg \tau \gg 0$:

$$\begin{aligned} R_{jk} &= \frac{\langle \eta_j(\rho; t, \vec{p})\, \mathcal{O}(\tau)\, \eta_k^\dagger(\rho; 0, \vec{p}) \rangle}{\sum_l \langle \eta_l(\rho; t, \vec{p}) \eta_l^\dagger(\rho; 0, \vec{p}) \rangle} \\ &= \frac{1}{2 + E^2/m^2} \, \frac{e^{-Et}}{e^{-Et} + e^{-E(T-t)}} T_{jk} \quad . \end{aligned} \tag{36}$$

For $T \gg \tau \gg t \gg 0$, we get an analogous equation with the additional sign factor from (31) and with $t$ replaced by $T - t$. For $t = T/2$, which is the choice in our numerical work, (36) gives

$$R_{jk} = \frac{1}{2 + E^2/m^2} \, \frac{1}{2} \, T_{jk} \quad . \tag{37}$$

The ratio may still depend on $\tau$ due to contributions from the higher states neglected in (29). By searching for plateaus in the $\tau$-dependence, one can extract the value of the ratio with the smallest contamination from higher states.

In the case of the pion, there is no polarization, and the relation (37) reduces to

$$R = \frac{\langle \pi; \vec{p} | \hat{O} | \pi; \vec{p} \rangle}{2} \quad . \tag{38}$$

# 4 Evaluation of three-point functions on the lattice

The actual form of the three-point correlator is given by

$$\langle \eta_\Gamma^F(t, \vec{p})\, \mathcal{O}^G(\tau)\, \eta_{\Gamma'}^{F'}(0, -\vec{p}) \rangle \quad . \tag{39}$$

Here we explicitly indicate the flavor matrices $F$, $F'$, and $G$. $\eta_\Gamma^F(t, \vec{p})$ is a meson operator with momentum $\vec{p}$ at time $t$:

$$\eta_\Gamma^F(t, \vec{p}) = \sum_{x: x_4 = t} e^{-\mathrm{i}\vec{p}\cdot\vec{x}}\, F_{ff'}\, \bar{\psi}^a_{f\alpha}(x) \Gamma_{\alpha\beta} \psi^a_{f'\beta}(x) \tag{40}$$

($a$ color, $f$ flavor, $\alpha$ Dirac index) with a suitably chosen Dirac matrix $\Gamma$. In the case of the rho, $\Gamma = \gamma_j$, while for the pion $\Gamma = \gamma_5$. A second meson operator is set at time slice 0 with momentum $-\vec{p}$, and $F' = F^\dagger$. The operator $\mathcal{O}^G(\tau)$ has the general form

$$\mathcal{O}^G(\tau) = \sum_{x, z, z': x_4 = \tau} G_{ff'}\, \bar{\psi}^a_{f\alpha}(z) J^{ab}_{\alpha\beta}(z, z'; x) \psi^b_{f'\beta}(z') \tag{41}$$

where $J^{ab}_{\alpha\beta}(z, z'; x)$ is a matrix that represents the flavor, Dirac, and derivative structure of the corresponding local operator. $x$ can be imagined as the "center of mass" of the operator while the sum over $z$ and $z'$ represents the derivative structure.

Inserting these definitions, the correlation function is

$$\begin{aligned} & \langle \eta_\Gamma^F(t, \vec{p})\, \mathcal{O}^G(\tau)\, \eta_{\Gamma'}^{F'}(0, -\vec{p}) \rangle \\ = \; & V_3 \sum_{x: x_4 = \tau} \sum_{y: y_4 = t} \sum_{z, z'} e^{-\mathrm{i}(\vec{p}\cdot\vec{y})}\, F_{fg}\, F'_{f'g'}\, G_{hh'}\, \Gamma_{\alpha\beta}\, \Gamma'_{\alpha'\beta'} \\ & \times \langle J^{bc}_{\gamma\delta}(z, z'; x)\, \bar{\psi}^a_{f\alpha}(y) \psi^a_{g\beta}(y)\, \bar{\psi}^b_{h\gamma}(z) \psi^c_{h'\delta}(z')\, \bar{\psi}^{a'}_{f'\alpha'}(0) \psi^{a'}_{g'\beta'}(0) \rangle \end{aligned} \tag{42}$$

where $V_3$ is the volume of a time slice.

We integrate out the fermion fields in the quenched approximation and define

$$\langle \psi^a_{f\alpha}(x) \bar{\psi}^b_{f'\beta}(y) \rangle_{\text{fermions}} = \delta_{ff'} G^{ab}_{\alpha\beta}(U|x,y) \tag{43}$$

where $G(U|x,y)$ is the fermion propagator in the gauge field configuration $U$ (the $U$ dependence will be indicated explicitly only when needed), and the average is over fermion fields. There are six different contraction terms. In four of them, two operators at the same location are contracted. These fermion line disconnected contributions are proportional to $\mathrm{tr}\, F$, $\mathrm{tr}\, F'$, and $\mathrm{tr}\, G$ and vanish if these matrices are chosen traceless. However, this is in general impossible for $\mathrm{tr}\, G$, as we shall see below, and the omission of the corresponding contraction must be regarded an approximation, which is however consistent with quenching. We use this approximation for the same reason we use quenching: it is very hard to go beyond it. The remaining two terms are the fermion line connected contributions

$$\begin{aligned} & -V_3 \sum_{x:x_4=\tau} \sum_{y:y_4=t} \sum_{z,z'} e^{-\mathrm{i}\vec{p}\cdot\vec{y}} \\ & \Big\langle (\mathrm{tr}\, FGF')\ \mathrm{tr}_{DC}\, (\Gamma G(y,z) J(z,z';x) G(z',0) \Gamma' G(0,y)) \\ & + (\mathrm{tr}\, F'GF)\ \mathrm{tr}_{DC}\, (\Gamma G(y,0) \Gamma' G(0,z) J(z,z';x) G(z',y)) \Big\rangle_g \end{aligned} \tag{44}$$

where the traces are over Dirac and color indices, and the average is over the gauge field alone.

The two terms can be related to each other by means of the following relations

$$G(x,y)^\dagger = \gamma_5 G(y,x) \gamma_5 \tag{45}$$

$$\gamma_5 \Gamma = s \Gamma^\dagger \gamma_5 \tag{46}$$

$$\gamma_5 \Gamma' = s' \Gamma'^\dagger \gamma_5 \tag{47}$$

$$\gamma_5 J(z,z';x)^\dagger \gamma_5 = s_J J(z',z;x) \tag{48}$$

where $s, s', s_J = \pm 1$, and eq. (48) is valid only if the correspondig operator is suitably symmetrized in its space-time indices. For the pion, $\Gamma = \Gamma' = \gamma_5$ and thus $s = s' = 1$, while for the rho, $\Gamma, \Gamma' \in \{\gamma_1, \gamma_2, \gamma_3\}$ and $s = s' = -1$. Then the correlation function reduces to

$$-V_3 \sum_{x:x_4=\tau} \sum_{y:y_4=t} e^{-\mathrm{i}\vec{p}\cdot\vec{y}} \left[ (\mathrm{tr}\, FGF') M(x,y) + s s' s_J\, (\mathrm{tr}\, F'GF)\, M(x,y)^* \right] \tag{49}$$

with the basic single-flavor correlation function

$$M(x,y) = \sum_{z,z'} \langle \mathrm{tr}_{DC}\, \Gamma G(y,z) J(z,z';x) G(z',0) \Gamma' G(0,y) \rangle_g \quad . \tag{50}$$

Note that the calculation of this quantity on the lattice requires only two inversions of the fermion matrix, one at 0 and one at $y$ or $z$.

Using the charge conjugation matrix, defined by

$$\gamma_\mu^T = -C^{-1} \gamma_\mu C \quad , \tag{51}$$

and the relations

$$\begin{aligned} G(U|x,y) &= C\, G(U^*|y,x)^T\, C^{-1} && (52)\\ C\Gamma^T C^{-1} &= \sigma \Gamma && (53)\\ C\Gamma'^T C^{-1} &= \sigma' \Gamma' && (54)\\ C J(U^*|z',z;x)^T C^{-1} &= \sigma_J J(U|z,z';x) && (55) \end{aligned}$$

(where we explicitly denoted the dependence of $J$ on the gauge field) with $\sigma, \sigma', \sigma_J = \pm 1$ one can further show that

$$M(x,y)^* = \sigma \sigma' \sigma_J\, s s' s_J\, M(x,y) \quad . \tag{56}$$

We choose traceless matrices for $F$ and $F'$,

$$F = \begin{pmatrix} 0 & 1 \\ 0 & 0 \end{pmatrix} \quad , \qquad F' = \begin{pmatrix} 0 & 0 \\ 1 & 0 \end{pmatrix} \quad , \tag{57}$$

and therefore

$$\mathrm{tr}\, F' G F = G_{11} \quad , \qquad \mathrm{tr}\, F G F' = G_{22} \quad . \tag{58}$$

We finally arrive at the following expression relating the propagators $M(x,y)$ to the three-point correlation function:

$$\begin{aligned} &\langle \eta_\Gamma^F(t,\vec{p})\, \mathcal{O}^G(\tau)\, \eta_{\Gamma'}^{F'}(0,-\vec{p}) \rangle = \\ &\quad = \; -V_3\, (G_{11} + \sigma_J\, G_{22}\,) \times \sum_{x:x_4=\tau} \sum_{y:y_4=t} e^{-\mathrm{i}\vec{p}\cdot\vec{y}}\, M(x,y) \end{aligned} \tag{59}$$

For an operator with $n$ derivatives, $\sigma_J$ is $(-1)^{n+n_5+1}$, where $n_5 = 1$ if the operator contains a $\gamma_5$ matrix, $n_5 = 0$ otherwise. Thus, for odd $n + n_5$, $G$ must not be traceless.

The analogous expression for the two-point correlation function reads

$$\begin{aligned} &\langle \eta_\Gamma^F(t,\vec{p})\, \eta_{\Gamma'}^{F'}(0,-\vec{p}) \rangle = \\ &\quad = \; -V_3 \sum_{x:x_4=t} e^{-\mathrm{i}\vec{p}\cdot\vec{x}} \langle \mathrm{tr}_{DC}\, G(x,0) \Gamma' G(0,x) \Gamma \rangle_g \quad . \end{aligned} \tag{60}$$

# 5 Lattice and continuum operators

Eqs. (36) and (38) relate the numerically computable ratios $R_{ij}$ and $R$ to expectation values of Euclidean lattice operators. To connect them with the corresponding continuum Minkowski-space operators, we first introduce the continuum matrix element of the renormalized Euclidean operator $\hat{O}_{\rm r}^{\rm cont}$ by the relation

$$Z_{\hat{O}}\,\langle\vec{p}\lambda|\hat{O}|\vec{p}\lambda\rangle = \frac{1}{2E(\vec{p})}\,\frac{1}{2\kappa}\,{}^{\rm cont}\langle\vec{p}\lambda|\hat{O}_{\rm r}^{\rm cont}|\vec{p}\lambda\rangle^{\rm cont} \quad . \tag{61}$$

The factor $2E(\vec{p})$ is a consequence of the different normalization on the lattice and in the continuum:

$$\begin{aligned} \langle\vec{p}\lambda|\vec{p}\,'\lambda'\rangle &= \delta_{\vec{p},\vec{p}\,'}\,\delta_{\lambda,\lambda'} \\ {}^{\rm cont}\langle\vec{p}\lambda|\vec{p}\,'\lambda'\rangle^{\rm cont} &= (2\pi)^3\,2E(\vec{p})\,\delta_{\lambda,\lambda'}\,\delta(\vec{p}-\vec{p}\,') \quad , \end{aligned} \tag{62}$$

and $2\kappa$ comes from the definition of the Wilson fermion action on the lattice. $Z_{\hat{O}}$ is the renormalization constant of the operator $\hat{O}$.

In the following, we shall use the renormalization constants calculated in one-loop lattice perturbation theory in the chiral limit [10]. They can be written in the form

$$Z_{\hat{O}} = 1 - \frac{g^2}{16\pi^2}\,C_F\,\left(\gamma_{\hat{O}}\ln(a\mu) + B_{\hat{O}} - B_{\hat{O}}^{\rm c}\right) , \tag{63}$$

where $C_F = 4/3$, $g$ denotes the bare coupling constant, and $\mu$ is the renormalization scale. Note that here the lattice spacing $a$ has been introduced explicitly. The finite contribution $B_{\hat{O}}$ is fixed in the momentum subtraction renormalization scheme, whereas $B_{\hat{O}}^{\rm c}$ represents the contribution of the continuum operator in the $\overline{\rm MS}$ scheme with an anticommuting $\gamma_5$. Hence multiplication by $Z_{\hat{O}}$ leads from bare operators on the lattice to the corresponding renormalized (in the $\overline{\rm MS}$ scheme) operators in the Euclidean continuum. For the renormalization scale $\mu$ we choose the inverse lattice spacing $a^{-1}$. Taking the physical rho mass of 770 MeV as input, we obtain from the lattice masses extrapolated to the chiral limit the value $\mu = 2.4\,{\rm GeV}$.

# 6 Results

We have collected more than 500 independent configurations on a $32 \times 16^3$ lattice at $\beta = 6.0$ with Wilson fermions and $r = 1$. Three different hopping parameters, $\kappa = 0.1515$, 0.153, and 0.155 were used. They correspond

to quark masses of roughly 190, 130 and 70 MeV, respectively. As in [2], each gauge update consisted of a single 3-hit Metropolis sweep followed by 16 overrelation sweeps. This cycle is repeated 50 times to generate a new configuration. The code was run on a Quadrics QH2 data-parallel computer. For completeness, the smearing technique – Jacobi smearing – we use to improve the overlap of the operator with the state is described in Appendix C.

The calculational procedure is as follows: We calculate in each configuration the three-point functions (50) for a large set of operators as well as the pion and rho two-point functions. In Appendix B we list the operators we have actually studied. Those without $\gamma_5$ are labeled by the pion moments $v_n$ one can compute from them. The expectation value of such an operator $\hat{O}_{v_n}$ in the rho is a linear combination of $a_n$ and $d_n$. The operators with $\gamma_5$ are labeled by the corresponding rho matrix elements $r_n$.

Using two values of the momentum, namely $\vec{p} = (0,0,0)$ and $\vec{p} = (\frac{2\pi}{16},0,0)$, we can check the continuum dispersion relation of the one-particle energies extracted from the two-point function. It is satisfied to better than 1%, and even for nonzero momentum we have a good projection on the ground state pion and rho. The particle masses we have used in our subsequent analysis are taken from Ref. [11]. They are collected in Table 1.

For the computation of the three-point functions, the locations of the source and the sink are held fixed at 0 and $t = T/2 = 16$. Placing the sink at $T/2$ allows us to search for a plateau equally well on both sides of the sink. In the case of the rho, we restrict ourselves to the 3–3 and 3–2 components.

For the denominator of the ratios we employed two different procedures: first, we took the actual value of the propagator at midpoint, and second, we fitted the interior 24 points of the propagator to exponential functions and used the resulting midpoint value. The second case resulted in somewhat smaller errors at certain values of $\kappa$ and $p^1$. We quote our results including the uncertainty from the former procedure. We also tried to use the conserved vector current, as proposed by [1], but this did not reduce our error margins.

The ratios (36) and (38) are taken as a function of the operator insertion point $\tau$, and a fit to the central 7 points on each side that make up the plateau is made. The full covariance matrix is considered in estimating the error, thus taking correlations between neighboring points into account (in fact, only about 2 independent degrees of freedom out of 7 survived). Some example plots are shown in Figs. 1 and 2.

In a few cases we have two operators for the same reduced continuum

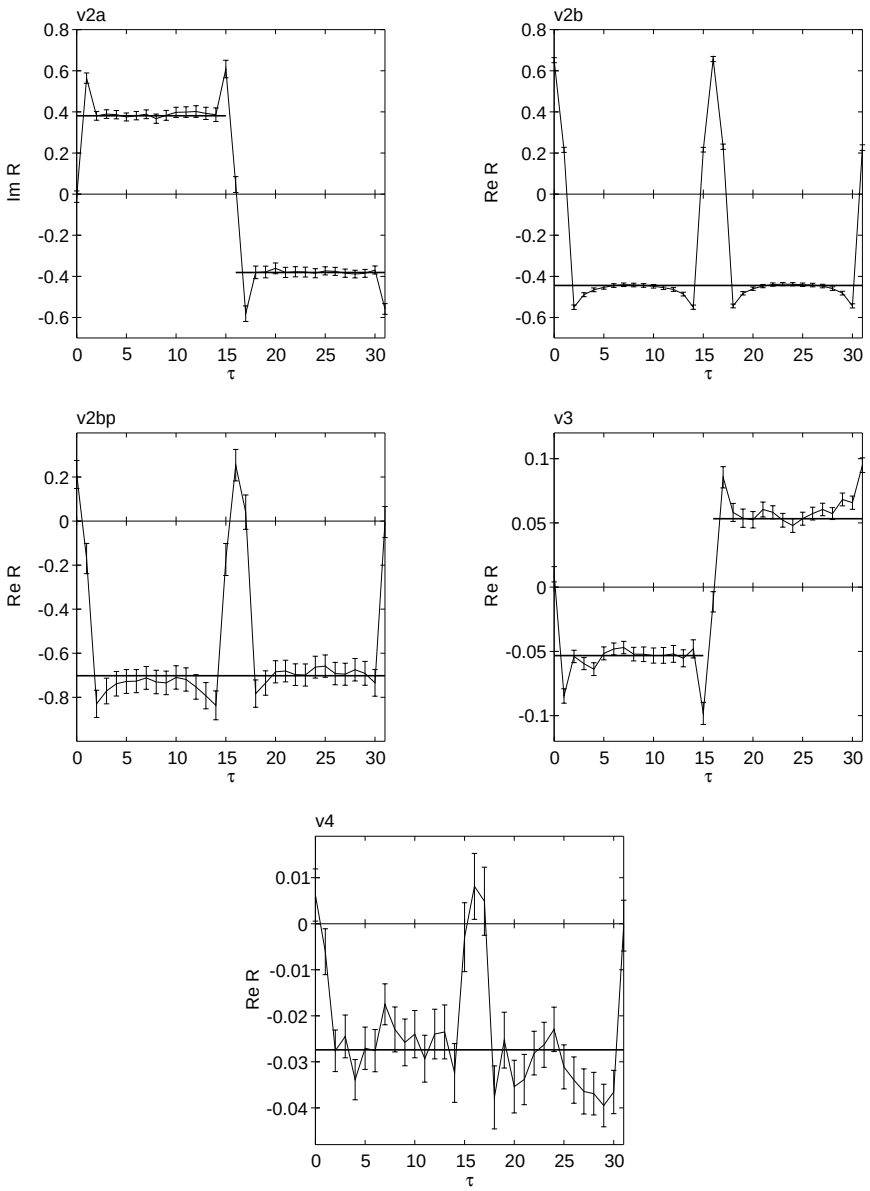


Figure 1: The ratio $R$ for the operators $\hat{O}_{v2a}$, $\hat{O}_{v2b}$, $\hat{O}_{v2b}$ at $\vec{p} \neq \vec{0}$, $\hat{O}_{v3}$, and $\hat{O}_{v4}$ (left to right, top to bottom) for the pion at $\kappa = 0.153$. The horizontal line is a fit to the central seven points on both sides.

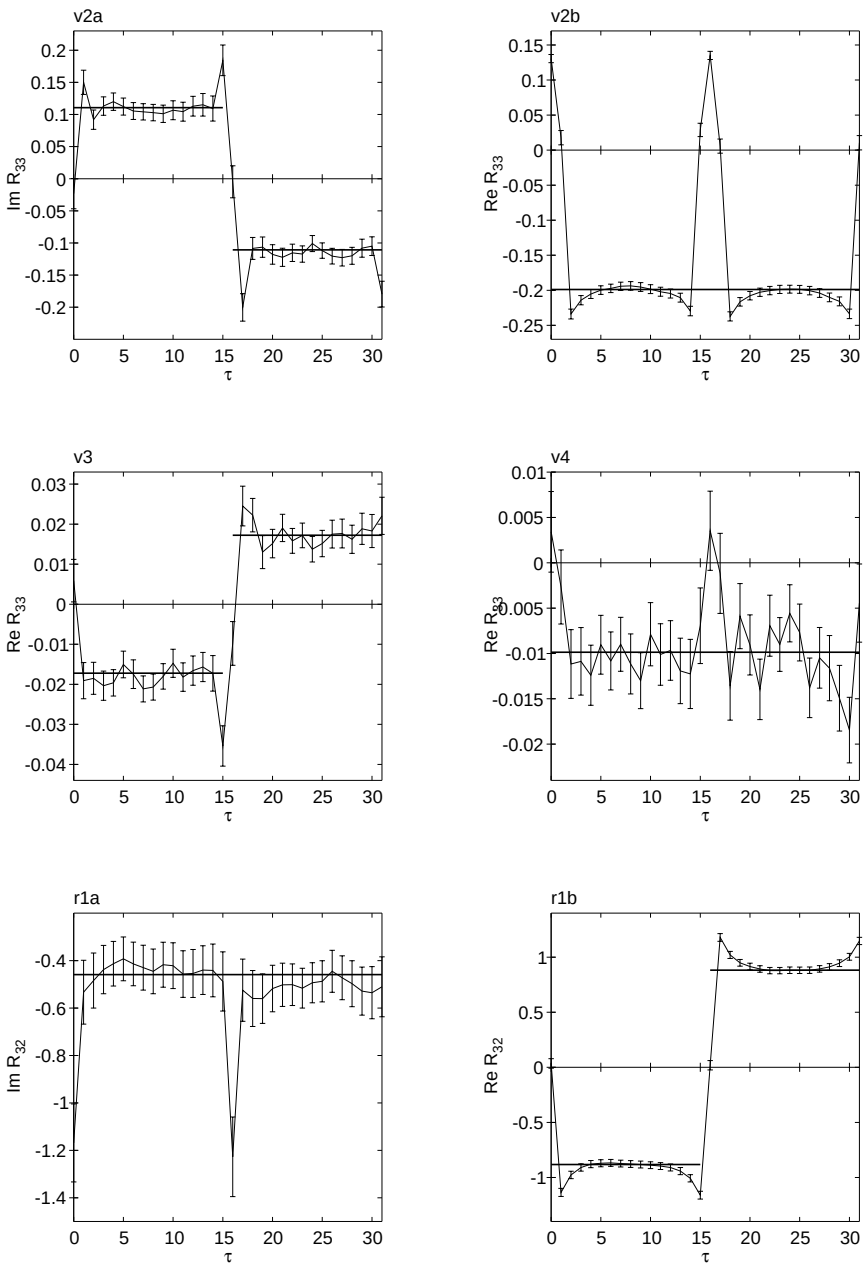


Figure 2: The ratios $R_{33}$ and $R_{32}$ for the rho operators $\hat{O}_{v2a}$, $\hat{O}_{v2b}$, $\hat{O}_{v3}$, $\hat{O}_{v4}$, $\hat{O}_{r1a}$, and $\hat{O}_{r1b}$ (left to right, top to bottom) at $\kappa = 0.153$.

| | $\kappa = 0.1515$ | $\kappa = 0.153$ | $\kappa = 0.155$ | $\kappa = \kappa_c = 0.15717(3)$ |
|---|---|---|---|---|
| Pion | 0.5033(4) | 0.4221(4) | 0.2966(5) | 0 |
| Rho | 0.5682(7) | 0.5058(8) | 0.4227(15) | 0.328(5) |

Table 1: Pion and rho masses in lattice units.

matrix element, distinguished by the subscripts $a$ and $b$. $\hat{O}_{v2,a}$ and $\hat{O}_{v2,b}$ as well as $\hat{O}_{r2,a}$ and $\hat{O}_{r2,b}$ belong to different representations of the hypercubic group $H(4)$. Hence the results extracted from operator $a$ and operator $b$ have to agree only in the continuum limit where the full $O(4)$ symmetry is hopefully restored, and a comparison of our results obtained for finite lattice spacing gives us some indication of the size of lattice artifacts. In the case of the operators associated to $v_{2,b}$, $r_{1,b}$, and $r_{2,a}$ we denote the results obtained with nonzero momentum by an additional subscript $p$.

Applying (38), (61), (76), and (78) we have calculated estimates for the pion moments $v_n$ from the measured ratios $R$. The results are summarized in Fig. 3 and in Table 2. The agreement (within errors) of $v_{2,a}$ and $v_{2,b}$ indicates that – at least in this case – lattice artifacts are not too large. Assuming a linear dependence on $1/\kappa$, i.e. on the bare quark mass, the values have been extrapolated to the chiral limit $\kappa = \kappa_c = 0.15717(3)$. Since the quark masses in our simulation are rather large ($> 70$MeV) we need this extrapolation in order to obtain numbers that can sensibly be compared with phenomenological valence quark distributions. Note, however, that the quark mass dependence of the results is not very pronounced. Only $v_{2,b}$ shows a significant trend towards smaller values as the chiral limit is approached which is the expected behavior.

We now come to the rho results (see Figs. 4, 5 and Table 2). By means of (32), (33), (61), and (76) we pass from the ratios (37) to matrix elements whose relation to $a_n$, $d_n$, and $r_n$ is listed in Eq. (79). The extrapolation to the chiral limit is performed as for the pion. In the case of the operators without $\gamma_5$, i.e. those labeled by $v_n$, we encounter the problem that instead of one number ($v_n$) we have to extract the two quantities $a_n$ and $d_n$ from the matrix elements.

Therefore we proceed as follows: The expectation value of $\hat{O}_{v2,b}$ at $\vec{p} = \vec{0}$ gives us directly $a_2$, and $d_2$ can then be calculated from $\hat{O}_{v2,a}$ and $\hat{O}_{v2,b}$ at nonvanishing momentum. The expectation values of $\hat{O}_{v3}$ and $\hat{O}_{v4}$, on the other hand, are proportional to $d_3$ and $d_4$, respectively, if $\vec{p} = \vec{0}$. With $d_3$

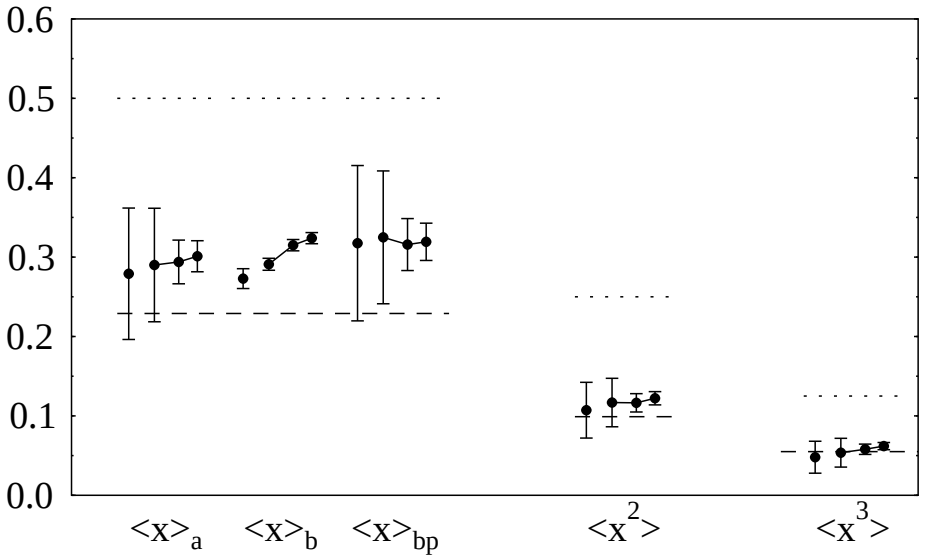


Figure 3: Estimates of the pion moments $v_n = \langle x^{n-1} \rangle$ for a single flavor. For each matrix element, the results from the three different $\kappa$ values are shown versus $1/\kappa$ with $\kappa$ decreasing (i.e. with the quark mass increasing) from left to right. The leftmost value is the chiral extrapolation obtained from a linear fit. The dotted lines give the free-field (heavy quark) limits. The dashed lines are phenomenological valence quark values from [3], evaluated at $\mu = 2.4\,\mathrm{GeV}$.

and $d_4$ computed from these matrix elements we use the corresponding results for $\vec{p} \neq \vec{0}$ to calculate $a_3$ and $a_4$.

From the matrix elements of the operators with $\gamma_5$ we can easily extract $r_1$, $r_2$, and $r_3$. The estimates $r_{2,a}$, $r_{2,ap}$, and $r_{2,b}$ for $r_2$ agree within the errors. Thus also in this case we do not observe significant discretization effects.

# 7 Discussion

We have calculated the lowest three moments of the structure functions of the pion and the rho meson, restricting ourselves to the leading twist-2 operators in the operator product expansion.

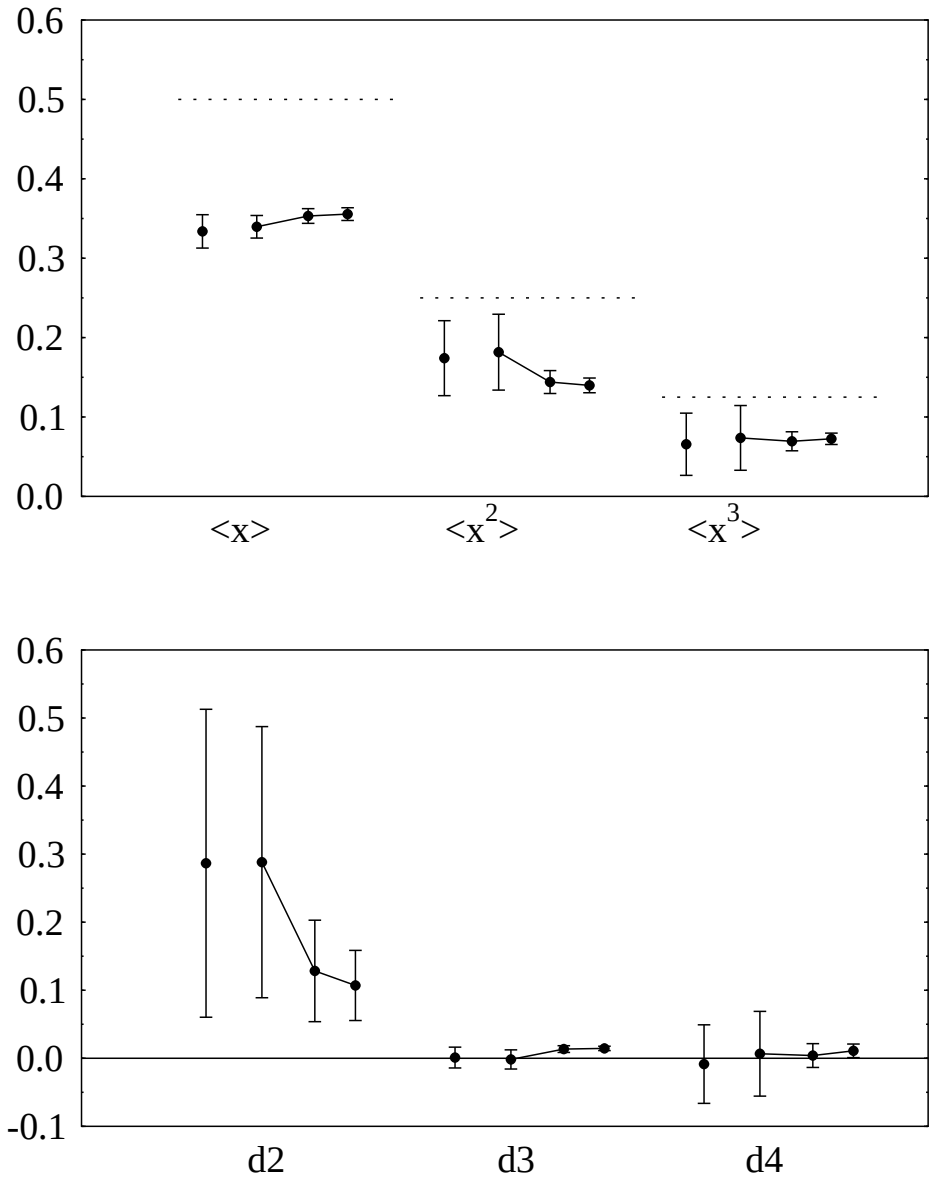


Figure 4: Estimates for the rho moments $a_n = \langle x^{n-1} \rangle$ and $d_n$. The presentation of the data is the same as in Fig. 3.

| | $\kappa = 0.1515$ | $\kappa = 0.153$ | $\kappa = 0.155$ | $\kappa = \kappa_c = 0.15717$ |
|---|---|---|---|---|
| PION | | | | |
| $v_{2,a} = \langle x \rangle_a$ | 0.301(20) | 0.294(28) | 0.290(71) | 0.279(83) |
| $v_{2,b} = \langle x \rangle_b$ | 0.3239(70) | 0.3150(71) | 0.2910(75) | 0.273(12) |
| $v_{2,bp} = \langle x \rangle_{bp}$ | 0.319(23) | 0.316(33) | 0.325(84) | 0.318(98) |
| $v_3 = \langle x^2 \rangle$ | 0.1222(83) | 0.116(12) | 0.117(31) | 0.107(35) |
| $v_4 = \langle x^3 \rangle$ | 0.0619(45) | 0.0580(65) | 0.054(18) | 0.048(20) |
| RHO | | | | |
| $a_2 = \langle x \rangle$ | 0.3555(80) | 0.3531(93) | 0.340(14) | 0.334(21) |
| $a_3 = \langle x^2 \rangle$ | 0.1398(93) | 0.144(14) | 0.182(48) | 0.174(47) |
| $a_4 = \langle x^3 \rangle$ | 0.0725(72) | 0.069(12) | 0.074(41) | 0.066(39) |
| $d_2$ | 0.107(52) | 0.128(75) | 0.29(20) | 0.29(23) |
| $d_3$ | 0.0145(32) | 0.0135(49) | $-0.002(14)$ | 0.001(15) |
| $d_4$ | 0.0109(100) | 0.004(17) | 0.007(62) | $-0.009(58)$ |
| $r_{1,a}$ | 0.709(56) | 0.715(97) | 0.42(34) | 0.57(32) |
| $r_{1,b}$ | 0.721(17) | 0.702(20) | 0.627(32) | 0.590(46) |
| $r_{1,bp}$ | 0.680(56) | 0.62(13) | 0.32(44) | 0.33(42) |
| $r_{2,a}$ | 0.2743(62) | 0.2631(70) | 0.231(12) | 0.212(17) |
| $r_{2,ap}$ | 0.257(17) | 0.243(25) | 0.216(69) | 0.198(76) |
| $r_{2,b}$ | 0.242(20) | 0.232(30) | 0.210(89) | 0.199(95) |
| $r_3$ | 0.1067(71) | 0.099(11) | 0.087(33) | 0.077(34) |

Table 2: Result overview for a single flavor. The numbers refer to the $\overline{\text{MS}}$ scheme with a renormalization scale $\mu \approx 2.4\,\text{GeV}$. The last column gives the result of the extrapolation to the chiral limit.

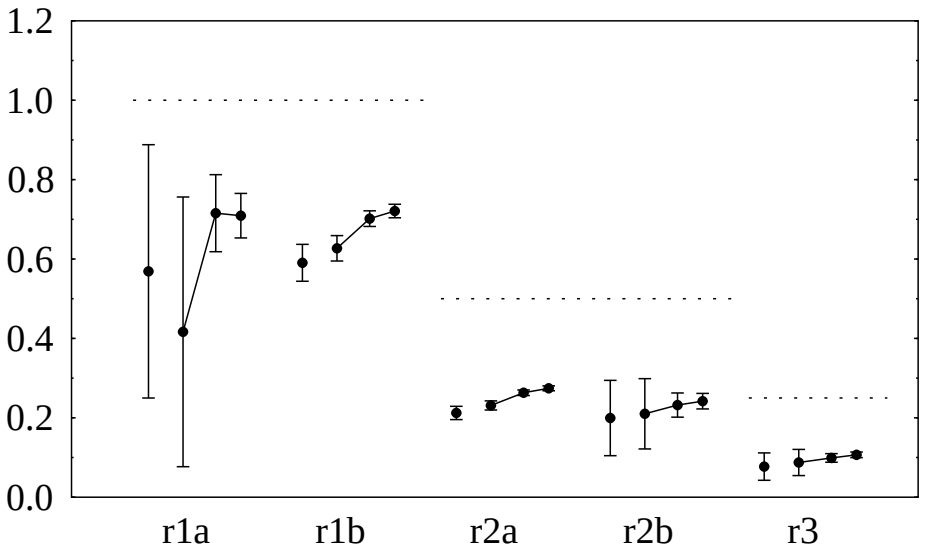


Figure 5: Estimates for the rho moments $r_n$. The presentation of the data is the same as in Fig. 3.

For the pion, we can compare our numbers in the chiral limit with the experimental data [3]. Our result for $\langle x \rangle$ is larger than phenomenology suggests. This is to be expected as our quenched lattice calculation does not contain any sea quarks and the valence quarks will therefore carry more of the momentum. The results for $\langle x^2 \rangle$ and $\langle x^3 \rangle$, on the other hand, are consistent with the phenomenological numbers. Our results also agree with the early lattice calculations of Martinelli and Sachrajda [1] as well as with various model calculations [12].

The unpolarized rho structure function looks very similar to the pion structure function, at least for the quark masses that we have considered. In the pion the quarks carry about 60% of the total momentum, while in the rho they carry about 70% at the smallest quark mass. The higher moments are in agreement with each other within the error bars. Thus the assumption $F_1^\rho(x) \sim F_1^\pi(x)$ often used in phenomenological estimates may well be justified.

The lowest moment $r_1$ of the polarized structure function $g_1$ indicates that the valence quarks carry about 60% of the total spin of the rho. For comparison, a similar quenched calculation for the nucleon gave a quark spin

fraction of about the same value [2], which is reduced to 18% by sea quark contributions [13]. It is very likely that the same will also happen here.

The structure functions $b_1, b_2$ measure the difference in quark distributions of a (spin projected) $m = 1$ and $m = 0$ rho meson. If the quarks were in a relative $s$-wave state in the infinite momentum frame, we would expect $b_1, b_2$ to be zero. The lowest moment $d_2$ turns out to be positive and surprisingly large on the scale of $a_2$, albeit with large statistical errors. Perhaps this indicates that the valence quarks have a substantial orbital angular momentum. This could also explain a relatively small quark spin fraction.

# Acknowledgements

This work was supported in part by the Deutsche Forschungsgemeinschaft. The numerical calculations were performed on the Quadrics parallel computer at Bielefeld University. We wish to thank the computer center for its help. C.B. thanks the Studienstiftung des Deutschen Volkes for its support.

# A Conventions

The Minkowski space metric has the signature $(1, -1, -1, -1)$. Minkowski and Euclidean components are related by

$$x_4 = \mathrm{i}x^{(M)0} = \mathrm{i}x_0^{(M)} \quad , \qquad x_j = x^{(M)j} = -x_j^{(M)} \quad , \tag{64}$$

where $j$ refers to spatial indices. Unless explicitly mentioned, we label Minkowski-space variables by an $(M)$.

Covariant derivatives are defined in Minkowski space as

$$D^{(M)\mu} = \partial^{(M)\mu} - \mathrm{i}gA^{(M)\mu} \tag{65}$$

and are related to their Euclidean counterparts as follows:

$$\mathrm{i}D^{(M)0} = -D_4 \quad , \qquad \mathrm{i}D^{(M)j} = -\mathrm{i}D_j \quad , \tag{66}$$

similarly for the gamma matrices:

$$\gamma^{(M)0} = \gamma_4 \quad , \qquad \gamma^{(M)j} = \mathrm{i}\gamma_j \quad . \tag{67}$$

The $\gamma_5$ matrix is defined as

$$\begin{aligned} \gamma_5^{(M)} &= \mathrm{i}\gamma^{(M)0}\gamma^{(M)1}\gamma^{(M)2}\gamma^{(M)3} \\ \gamma_5 &= \gamma_1\gamma_2\gamma_3\gamma_4 = -\gamma_5^{(M)} \quad . \end{aligned} \tag{68}$$

The momentum of the particles is chosen in the 1-direction, $\vec{p} = (p, 0, 0)$. Polarization vectors for vector particles satisfy

$$p^{(M)\mu}\epsilon_\mu^{(M)}(\vec{p},\lambda) = 0 \quad , \qquad \epsilon^{(M)\mu}(\vec{p},\lambda)\epsilon_\mu^{(M)}(\vec{p},\lambda') = -m^2\,\delta_{\lambda\lambda'} \tag{69}$$

$(\lambda = \pm, 0)$ and have the explicit form

$$\epsilon^{(M)\mu}(\vec{p},\lambda) = \left(\frac{\vec{p}\cdot\vec{e}_\lambda}{m}, \vec{e}_\lambda + \frac{\vec{p}\cdot\vec{e}_\lambda}{m(m+E)}\vec{p}\right) \tag{70}$$

with the basis vectors

$$\vec{e}_\pm = \mp\frac{m}{\sqrt{2}}\,(0, 1, \pm\mathrm{i}) \tag{71}$$

$$\vec{e}_0 = m\,(1, 0, 0) \quad . \tag{72}$$

They satisfy the completeness relation

$$\sum_\lambda \epsilon_i^{(M)*}(\vec{p},\lambda)\epsilon_j^{(M)}(\vec{p},\lambda) = m^2\left(\delta_{ij} + \frac{1}{m^2}p_i p_j\right) \quad . \tag{73}$$

Note that in Euclidean space $\epsilon_j(\vec{p},\lambda) = \epsilon^{(M)j}(\vec{p},\lambda)$.

# B Operators

On the lattice, the choice of the operators to look at is a nontrivial matter, because the discretization reduces the symmetry group of (Euclidean) space-time from $O(4)$ to the hypercubic group $H(4) \subset O(4)$. Hence the lattice operators have to be classified according to $H(4)$ and one should choose operators belonging to a definite irreducible representation of $H(4)$. Since $H(4)$ is a finite group, the restrictions imposed by symmetry are less stringent than in the continuum and the possibilities for mixing increase. Whereas mixing with operators of the same dimension is supposed to be treatable by perturbation theory, the mixing coefficients for lower-dimensional operators have to be calculated nonperturbatively. Hence one would like to avoid mixing with

| Operator $\hat{O}$ | $Z_{\hat{O}}$ |
|---|---|
| $\hat{O}_{v2,a}$ | 0.989196 |
| $\hat{O}_{v2,b}$ | 0.978369 |
| $\hat{O}_{v3}$ | 1.102397 |
| $\hat{O}_{v4}$ | 1.229911 |

| Operator $\hat{O}$ | $Z_{\hat{O}}$ |
|---|---|
| $\hat{O}_{r1,a}$, $\hat{O}_{r1,b}$ | 0.866625 |
| $\hat{O}_{r2,a}$ | 0.997086 |
| $\hat{O}_{r2,b}$ | 0.998587 |
| $\hat{O}_{r3}$ | 1.108573 |

Table 3: Renormalization constants $Z$.

lower-dimensional operators whenever possible. On the other hand, as the spin grows, operators with no mixing at all require more and more nonvanishing momentum components in the calculation of their forward hadronic matrix elements, which makes their Monte Carlo evaluation increasingly difficult. So some kind of compromise is needed.

Due to our use of the quenched approximation purely gluonic operators cannot mix with two-quark operators and we may restrict ourselves to the latter. Guided by their $H(4)$ classification given in Ref. [9] we have chosen the following operators in Euclidean space:

$$\begin{aligned}
\hat{O}_{v2,a} &= \hat{O}_{\{41\}} \quad , \\
\hat{O}_{v2,b} &= \hat{O}_{44} - \frac{1}{3}\left(\hat{O}_{11} + \hat{O}_{22} + \hat{O}_{33}\right) \quad , \\
\hat{O}_{v3} &= \hat{O}_{\{114\}} - \frac{1}{2}\left(\hat{O}_{\{224\}} + \hat{O}_{\{334\}}\right) \quad , \\
\hat{O}_{v4} &= \hat{O}_{\{1122\}} + \hat{O}_{\{3344\}} + \hat{O}_{\{1133\}} + \hat{O}_{\{2244\}} - 2\hat{O}_{\{1144\}} - 2\hat{O}_{\{2233\}} \quad , \\
\hat{O}_{r1,a} &= \hat{O}^5_4 \quad , \\
\hat{O}_{r1,b} &= \hat{O}^5_1 \quad , \\
\hat{O}_{r2,a} &= \hat{O}^5_{\{41\}} \quad , \\
\hat{O}_{r2,b} &= \hat{O}^5_{44} - \frac{1}{3}\left(\hat{O}^5_{11} + \hat{O}^5_{22} + \hat{O}^5_{33}\right) \quad , \\
\hat{O}_{r3} &= \hat{O}^5_{\{114\}} - \frac{1}{2}\left(\hat{O}^5_{\{224\}} + \hat{O}^5_{\{334\}}\right) \quad . \qquad (74)
\end{aligned}$$

For $v_2$ and $r_2$ we have two operators, which belong to the same $O(4)$ multiplet in the continuum limit but transform according to inequivalent representations of $H(4)$. Hence their matrix elements provide a test for the restoration of $O(4)$ symmetry. The renormalization constants for these operators in the $\overline{\rm MS}$ scheme are listed in Table 3.

Concerning the mixing properties a few remarks are in order. Mixing with operators of equal or lower dimension is excluded for the operators $\hat{O}_{v2,a}$, $\hat{O}_{v2,b}$, $\hat{O}_{r1,a}$, $\hat{O}_{r1,b}$, $\hat{O}_{r2,a}$, $\hat{O}_{r2,b}$. The case of the operator $\hat{O}_{v3}$, for which there are two further operators with the same dimension and the same transformation behavior, is discussed in ref. [9]. The operators $\hat{O}_{v4}$ and $\hat{O}_{r3}$, on the other hand, could in principle mix not only with operators of the same dimension but also with an operator of one dimension less and different chiral properties. It is of the type

$$\bar{\psi}\sigma_{\mu\nu}\gamma_5 \overleftrightarrow{D}_{\mu_1} \overleftrightarrow{D}_{\mu_2} \cdots \overleftrightarrow{D}_{\mu_n} \psi \,, \tag{75}$$

where $n = 2$ in the case of $\hat{O}_{v4}$, and $n = 1$ for $\hat{O}_{r3}$.

Our analysis ignores mixing completely. This seems to be well justified for $\hat{O}_{v3}$. Here a perturbative calculation gives a rather small mixing coefficient for one of the mixing operators, whereas the other candidate for mixing does not appear at all in a 1-loop calculation, because its Born term vanishes in forward matrix elements. The same is true for all operators of dimension less than or equal to six which transform identically to $\hat{O}_{v4}$: Their Born term vanishes in forward matrix elements, hence they do not show up in a 1–loop calculation. In the case of $\hat{O}_{r3}$, however, the mixing is already visible at the 1–loop level. The results for $v_4$ and $r_3$ have therefore to be considered with some caution.

The corresponding Minkowski operators are found by applying eq. (23). Defining the Minkowski analogs of our Euclidean operators by

$$\begin{aligned}
\hat{O}_{v2,a} &= \mathrm{i}\hat{O}^{(M)}_{v2,a} \,, & \hat{O}_{v2,b} &= -\hat{O}^{(M)}_{v2,b} \,, \\
\hat{O}_{v3} &= -\hat{O}^{(M)}_{v3} \,, & \hat{O}_{v4} &= \hat{O}^{(M)}_{v4} \,, \\
\hat{O}_{r1,a} &= -\hat{O}^{(M)}_{r1,a} \,, & \hat{O}_{r1,b} &= \mathrm{i}\hat{O}^{(M)}_{r1,b} \,, \\
\hat{O}_{r2,a} &= -\mathrm{i}\hat{O}^{(M)}_{r2,a} \,, & \hat{O}_{r2,b} &= \hat{O}^{(M)}_{r2,b} \,, \\
\hat{O}_{r3} &= \hat{O}^{(M)}_{r3} \,,
\end{aligned} \tag{76}$$

we have

$$\begin{aligned}
\hat{O}^{(M)}_{v2,a} &= \hat{O}^{(M)\{01\}} \,, \\
\hat{O}^{(M)}_{v2,b} &= \hat{O}^{(M)00} + \frac{1}{3}\left(\hat{O}^{(M)11} + \hat{O}^{(M)22} + \hat{O}^{(M)33}\right) \,, \\
\hat{O}^{(M)}_{v3} &= \hat{O}^{(M)\{110\}} - \frac{1}{2}\left(\hat{O}^{(M)\{220\}} + \hat{O}^{(M)\{330\}}\right) \,,
\end{aligned}$$

$$
\begin{aligned}
\hat{O}^{(M)}_{v4} &= -\hat{O}^{(M)\{1122\}} + \hat{O}^{(M)\{3300\}} - \hat{O}^{(M)\{1133\}} + \hat{O}^{(M)\{2200\}} \\
&\quad - 2\hat{O}^{(M)\{1100\}} + 2\hat{O}^{(M)\{2233\}} \quad , \\
\hat{O}^{(M)}_{r1,a} &= \hat{O}^{(M)0}_5 \quad , \\
\hat{O}^{(M)}_{r1,b} &= \hat{O}^{(M)1}_5 \quad , \\
\hat{O}^{(M)}_{r2,a} &= \hat{O}^{(M)\{01\}}_5 \quad , \\
\hat{O}^{(M)}_{r2,b} &= \hat{O}^{(M)00}_5 + \frac{1}{3}\left(\hat{O}^{(M)11}_5 + \hat{O}^{(M)22}_5 + \hat{O}^{(M)33}_5\right) \quad , \\
\hat{O}^{(M)}_{r3} &= \hat{O}^{(M)\{110\}}_5 - \frac{1}{2}\left(\hat{O}^{(M)\{220\}}_5 + \hat{O}^{(M)\{330\}}_5\right) \quad . \qquad (77)
\end{aligned}
$$

We can now use (13), (14), and (15) to calculate the expectation values of the Minkowski space operators. For the pion, one obtains with $p^2 = p^3 = 0$

$$
\begin{aligned}
\langle \hat{O}^{(M)}_{v2,a} \rangle &= 2v_2 p^0 p^1 \quad , \\
\langle \hat{O}^{(M)}_{v2,b} \rangle &= 2v_2 \left((p^0)^2 + \frac{1}{3}(p^1)^2\right) \quad , \\
\langle \hat{O}^{(M)}_{v3} \rangle &= 2v_3 (p^1)^2 p^0 \quad , \\
\langle \hat{O}^{(M)}_{v4} \rangle &= -4v_4 (p^1)^2 (p^0)^2 \quad . \qquad (78)
\end{aligned}
$$

For the rho with polarization $\lambda = \pm$, one finds

$$
\begin{aligned}
\langle \hat{O}^{(M)}_{v2,a} \rangle &= 2\left(a_2 - \frac{1}{3}d_2\right) p^0 p^1 \quad , \\
\langle \hat{O}^{(M)}_{v2,b} \rangle &= 2\left(a_2 - \frac{1}{3}d_2\right)\left((p^0)^2 + \frac{1}{3}(p^1)^2\right) + \frac{2}{3}m^2 d_2 \quad , \\
\langle \hat{O}^{(M)}_{v2,b} \rangle_{p^1=0} &= 2a_2 m^2 \quad , \\
\langle \hat{O}^{(M)}_{v3} \rangle &= 2\left(a_3 - \frac{1}{3}d_3\right)(p^1)^2 p^0 - \frac{1}{3}m^2 d_3 p^0 \quad , \\
\langle \hat{O}^{(M)}_{v4} \rangle &= -4\left(a_4 - \frac{1}{3}d_4\right)(p^1)^2 (p^0)^2 + \frac{1}{3}m^4 d_4 \quad , \\
\langle \hat{O}^{(M)}_{r1,a} \rangle &= \pm 2 r_1 p^1 \quad , \\
\langle \hat{O}^{(M)}_{r1,b} \rangle &= \pm 2 r_1 p^0 \quad , \\
\langle \hat{O}^{(M)}_{r2,a} \rangle &= \pm r_2 \left((p^0)^2 + (p^1)^2\right) \quad , \\
\langle \hat{O}^{(M)}_{r2,b} \rangle &= \pm \frac{8}{3} r_2 p^0 p^1 \quad , \\
\langle \hat{O}^{(M)}_{r3} \rangle &= \pm \frac{2}{3} r_3 p^1 \left((p^1)^2 + 2(p^0)^2\right) \quad . \qquad (79)
\end{aligned}
$$

# C Smearing

The method we use for smearing is to smear the quark in a plane $x_4 = t$ [14]:

$$ {}^S\psi^a_{f\alpha}(\vec{x},t) = \sum_{\vec{y}} {}^S H^{ab}(\vec{x},\vec{y};U,t)\psi^b_{f\alpha}(\vec{y},t)\,, \tag{80} $$

where the kernel $H$ is chosen to have the correct gauge transformation properties and is diagonal in spin space. $S$ is the smearing label. So for example for no smearing $S = L =$ local, then ${}^L H^{ab}(\vec{x},\vec{y};U,t) = \delta^{ab}\delta_{\vec{x}\vec{y}}$. ${}^S H$ is also taken as Hermitian:

$$ {}^S H^{ba}(\vec{y},\vec{x};U,t)^* = {}^S H^{ab}(\vec{x},\vec{y};U,t)\,. \tag{81} $$

Also the smeared anti-quark is defined as

$$ {}^S\bar{\psi}^a_{f\alpha}(\vec{x},t) = \sum_{\vec{y}} \bar{\psi}^b_{f\alpha}(\vec{y},t) H^{ba}_S(\vec{y},\vec{x};U,t)\,. \tag{82} $$

Note that we can choose different smearing for the quark and anti-quark. Thus for a smeared meson operator we have

$$ {}^{S'S}\eta(t,\vec{p}) = \sum_{\vec{x}} F_{ff'} e^{-\mathrm{i}\vec{p}\cdot\vec{x}}\, {}^{S'}\bar{\psi}^a_{f\alpha}(\vec{x},t)\Gamma_{\alpha\beta}\, {}^S\psi^a_{f'\beta}(\vec{x},t) \tag{83} $$

with the appropriate correlation function

$$ C^{S'S}(t,\vec{p};t_0) = \langle {}^{S'S'}\eta(t,\vec{p})\, {}^{SS}\eta(t_0,-\vec{p})\rangle \tag{84} $$

so that $S$ and $S'$ is smearing at the source, sink respectively.

The smeared quark propagator is defined by

$$ {}^{S'S}G^{fab}_{\alpha\beta}(x,y;U)\delta_{ff'} = \langle {}^{S'}\psi^a_{f\alpha}(x)\, {}^S\bar{\psi}^b_{f'\beta}(y)\rangle_{\text{fermions}} \tag{85} $$

(${}^{LL}G \equiv G$). So in meson correlation functions we can simply replace $G$ with ${}^{S'S}G$ to allow for smearing.

The smeared quark propagators are found sequentially:

- Generate the smeared source ${}^S S$ from a point source at $(\vec{x}_0,t_0)$ and so with $S^a_{0\alpha}(\vec{x}t) = \delta_{\vec{x}\vec{x}_0}\delta_{tt_0}\delta^{aa_0}\delta_{\alpha\alpha_0}$,

$$ {}^S S^{faa_0}_{\alpha\alpha_0}(\vec{x},t;\vec{x}_0,t_0) = {}^S H^{aa_0}(\vec{x},\vec{x}_0;U,t)\delta_{tt_0}\delta_{\alpha\alpha_0}\,. \tag{86} $$

- Find ${}^{LS}G$, by solving $M\,{}^{LS}G = {}^{S}S$. We thus have

$$ {}^{LS}G^{fab}_{\alpha\beta}(\vec{x},t;\vec{x}_0,t_0) \equiv \sum_{\vec{y}} G^{fab'}_{\alpha\beta}(\vec{x},t;\vec{y},t_0)\,{}^{S}H^{b'b}(\vec{y},\vec{x}_0;U,t_0)\,. \qquad (87) $$

- From ${}^{LS}G$ we generate ${}^{S'S}G$ by applying ${}^{S'}H$:

$$ {}^{S'S}G^{fab}_{\alpha\beta}(\vec{x},t;\vec{x}_0,t_0) = \sum_{\vec{y}} {}^{S'}H^{aa'}(\vec{x},\vec{y};U,t)\,{}^{LS}G^{fa'b}_{\alpha\beta}(\vec{y},t;\vec{x}_0,t_0)\,. \qquad (88) $$

  Note that this step can be expensive (in CPU time) in comparison to eq. (86) as we must smear on every $x_4 = t$ plane.

Practically we shall use Jacobi smearing (as advocated mainly by [15]). This is given by

$$ \sum_{\vec{x}'} K(\vec{x},t;\vec{x}'t)\,{}^{S}S(\vec{x}',t) = S_0(\vec{x},t)\,, \qquad (89) $$

where $S_0$ is the original point source. Here

$$ K = 1 - \kappa_s D_s \qquad (90) $$

and $D_s$ is a covariant derivative in the $x_4 = t$ plane, viz.

$$ D^{ab}_{s\alpha\beta}(\vec{x},t;\vec{y},t) = \delta_{\alpha\beta}\sum_{i=1}^{3}\left[U^{ab}_i(\vec{x},t)\delta_{\vec{x}+\vec{\imath},\vec{y}} + U^{\dagger ab}_i(\vec{x}-\vec{\imath},t)\delta_{\vec{x}-\vec{\imath},\vec{y}}\right]\,. \qquad (91) $$

Hence we need $H = K^{-1}$. Rather than performing this inversion completely we Jacobi iterate $N_s$ times, so

$$ {}^{S}S^{(n)}(\vec{x},t) = S_0(\vec{x},t) + \kappa_s D_s\,{}^{S}S^{(n-1)}(\vec{x},t) \qquad n = 1,2,\ldots \qquad (92) $$

with ${}^{S}S^{(0)}(\vec{x},t) = S_0(\vec{x},t)$.

We thus have two parameters, $\kappa_s$, $N_s$ at our disposal. $\kappa_s$ controls the coarseness of the iteration, while increasing $N_s$ increases the size of the smeared object roughly like a random walk. Physically we wish to smear until our source is about the size of the meson. A suitable measure of the (rms) radius is given by

$$ r^2 = \frac{\sum_{\vec{x}}(\vec{x}-\vec{x}_0)^2\left|{}^{S}S(\vec{x},t_0;\vec{x}_0,t_0)\right|^2}{\left|{}^{S}S(\vec{x},t_0;\vec{x}_0,t_0)\right|^2}\,. \qquad (93) $$

(Note that on a periodic lattice, $(\vec{x}-\vec{x}_0)^2$ is taken as the minimum distance from $\vec{x}$ to $\vec{x}_0$.) Explicitly for $\beta = 6.0$ we have chosen $\kappa_s = 0.21$, $N_s = 50$. This gives $ra$ of about $3.5a \gtrsim 0.5$fm which corresponds roughly to the hadron radius.

# References


[1] G. Martinelli and C. T. Sachrajda, Phys. Lett. B196, 184 (1987); Nucl. Phys. B306, 865 (1988).

[2] M. Göckeler, R. Horsley, E.-M. Ilgenfritz, H. Perlt, P. Rakow, G. Schierholz, and A. Schiller, Phys. Rev. D53, 2317 (1996).

[3] P. J. Sutton, A. D. Martin, R. G. Roberts, and W. J. Stirling, Phys. Rev. D 45, 2349 (1992).

[4] H1 Collaboration, paper pa02-063 submitted to the '28th International Conference on High Energy Physics ICHEP96', Warsaw, July 1996.

[5] N. S. Craigie and G. Schierholz, Nucl. Phys. B100, 125 (1975).

[6] H. Holtmann, G. Levman, N. N. Nikolaev, A. Szczurek, and J. Speth, Phys. Lett. B 338, 363 (1994).

[7] P. Hoodbhoy, R. L. Jaffe, and A. Manohar, Nucl. Phys. B312, 571 (1989).

[8] L. Mankiewicz, Phys. Rev. D40, 255 (1989).

[9] M. Göckeler, R. Horsley, E.-M. Ilgenfritz, H. Perlt, P. Rakow, G. Schierholz, and A. Schiller, Phys. Rev. D54, 5705 (1996).

[10] M. Göckeler, R. Horsley, E.-M. Ilgenfritz, H. Perlt, P. Rakow, G. Schierholz, and A. Schiller, Nucl. Phys. B472, 309 (1996).

[11] M. Göckeler, R. Horsley, H. Perlt, P. Rakow, G. Schierholz, A. Schiller, and P. Stephenson, Phys. Lett. B391, 388 (1997).

[12] T. Shigetani, K. Suzuki, and H. Toki, Phys. Lett. B308, 383 (1993); G. Altarelli, S. Petrarca, and F. Rapuano, Phys. Lett. B373, 200 (1996).

[13] R. Altmeyer, M. Göckeler, R. Horsley, E. Laermann, and G. Schierholz, Phys. Rev. D49, 3087 (1994); M. Fukugita, Y. Kuramashi, M. Okawa, and A. Ukawa, Phys. Rev. Lett. 75, 2092 (1995); S. J. Dong, J.-F. Lagaë, and K. F. Liu, Phys. Rev. Lett. 75, 2096 (1995).

[14] C. Alexandrou, S. Güsken, F. Jegerlehner, K. Schilling, and R. Sommer, Nucl. Phys. B414, 815 (1994).

[15] C. R. Allton et al., UKQCD Collaboration, Phys. Rev. D47, 5128 (1993).